ELSEVIER

Journal of Alloys and Compounds 293–295 (1999) 74–87

Journal of ALLOYS AND COMPOUNDS

Hydrogen ordering and H-induced phase transformations in Zr-based intermetallic hydrides

V.A. Yartys[a,b,*], H. Fjellvåg[a,c], I.R. Harris[d], B.C. Hauback[a], A.B. Riabov[b], M.H. Sørby[a,c], I.Yu. Zavaliy[b]

[a]*Institute for Energy Technology, P.O. Box 40, Kjeller N-2027, Norway*

[b]*Metal Hydrides Department, Karpenko Physico-Mechanical Institute of the National Academy of Sciences of Ukraine, 5, Naukova Str., Lviv 290601, Ukraine*

[c]*Department of Chemistry, University of Oslo, N-0315 Oslo, Norway*

[d]*School of Metallurgy and Materials, The University of Birmingham, Edgbaston, Birmingham B15 2TT, UK*

Abstract

Crystal chemistry aspects of hydrogen behaviour in the zirconium–iron intermetallic deuterides (hydrides), $Zr_2FeD_{1.80-5.00}$, $Zr_3FeD_{1.27-6.70}$ and $Zr_4Fe_2O_{0.6}H_{7.80}$, were studied with a focus on the application of high resolution powder neutron diffraction. The effects of crystal structure, chemical composition of the metal matrices, temperature and hydrogen contents on preferences in the interstices occupation and H ordering were investigated and discussed in relation to the H absorption–desorption properties. The Hydrogenation–Disproportionation–Desorption–Recombination process was successfully applied to all materials studied, including the first reported example of an oxygen-containing compound, $Zr_4Fe_2O_{0.6}$.

Keywords: Hydrides; Zirconium; Iron; Powder neutron diffraction; Crystal structure; Hydrogenation–Disproportionation–Desorption–Recombination

1. Introduction

Zirconium-containing alloys are attractive as hydrogen storage alloys (HSA), hydrogen getters and metal hydride battery electrode materials. Zirconium–iron HSA, and in particular Zr-rich alloys with more than 50 at.% Zr, meet the requirements of effective hydrogen getters. The ST 198 Zr–Fe alloy (SAES Getters) is one type of such a hydrogen getter which contains the Zr_2Fe intermetallic compound as its major constituent.

A number of publications describe hydrogenation properties of Zr–Fe intermetallics (Zr_2Fe [1–4], Zr_3Fe [5–7], $Zr_4Fe_2O_{0.6}$ [8,9], Zr_6FeAl_2 [10]). Dependent on the applied hydrogenation conditions, either hydrides of interstitial type or materials disproportionated into Zr dihydride can be formed on hydrogen absorption by the binary Zr_2Fe and Zr_3Fe intermetallics [1–7]. The irreversibility of the disproportionation of Zr_2Fe was pointed out in Ref. [2], and was considered to limit the performance of the material. However, recently the Hydrogenation–Disproportionation–Desorption–Recombination (HDDR) route was successfully applied to Zr_2Fe [4] and Zr_3Fe [7]. The route provides a complete recovery of the original intermetallic phase and its H-sorption characteristics. Furthermore, it provides the possibility to synthesise these compounds in a microcrystalline state which is favourable for H-storage applications.

Powder neutron diffraction studies of the saturated deuterides $Zr_2FeD_{5.0}$ [3], $Zr_3FeD_{6.7}$ [7] and $Zr_6FeAl_2D_{10}$ [10] showed completely ordered hydrogen sublattices with all D–D distances exceeding 2.0 Å. The deuterium atoms occupy interstices formed either exclusively by zirconium atoms (Zr_4-tetrahedra in $Zr_2FeD_{5.0}$, $Zr_3FeD_{6.7}$ and $Zr_6FeAl_2D_{10}$) or by zirconium and iron atoms (Zr_3Fe-tetrahedra in $Zr_2FeD_{5.0}$; Zr_3Fe-tetrahedra and Zr_3Fe_2 trigonal bipyramids in $Zr_3FeD_{6.7}$ and $Zr_6FeAl_2D_{10}$).

This work focuses on H-ordering and H-induced phase transformations in binary and ternary intermetallics formed by zirconium and iron, i.e., Zr_2Fe, Zr_3Fe and $Zr_4Fe_2O_{0.6}$, over a wide range of H/D contents in the metal matrices. Despite the rather small variation in Zr content of the metal matrices, ranging from 60.6 ($Zr_4Fe_2O_{0.6}$) to 75.0 at.% (Zr_3Fe), there are significant differences in their properties as hydrogen storage materials. This fact will be discussed in relation to characteristic features of the crystal

*Corresponding author. Tel.: +47-6380-6453; fax: +47-6381-0920.
E-mail address: VLAD@ife.no (V.A. Yartys)

0925-8388/99/$ – see front matter
PII: S0925-8388(99)00304-7

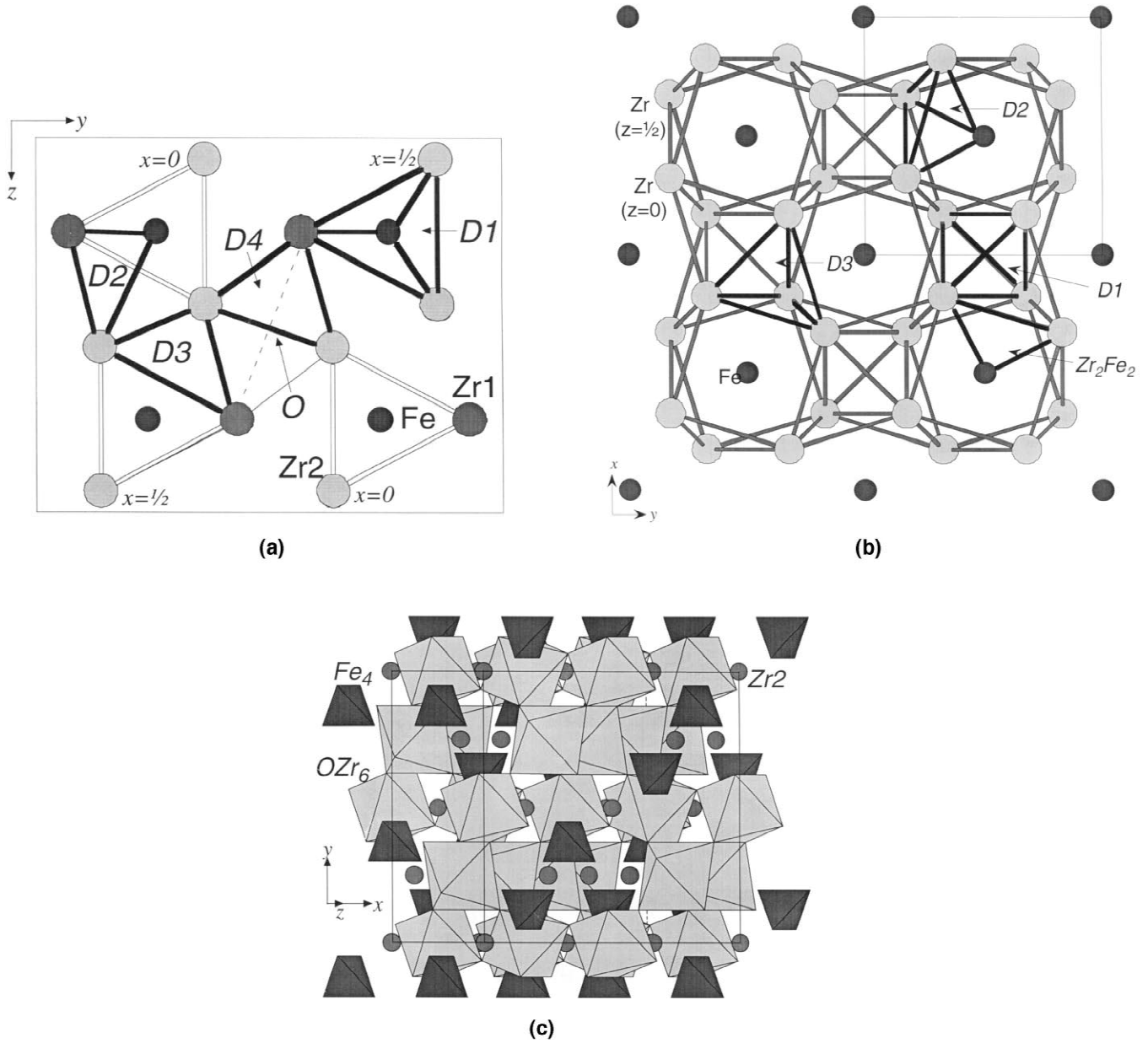

Fig. 1. (a) Crystal structure of Zr_3Fe (Re_3B type). Note Fe-centred Zr_6-trigonal prisms and the four types of interstices occupied by D atoms in $Zr_3FeD_{6.7}$: D1 (Zr_3Fe_2), D2 (Zr_3Fe), D3 (Zr_4) and D4 (Zr_4). (b) Crystal structure of Zr_2Fe ($CuAl_2$ type). Note Fe-centred Zr_8-tetragonal antiprisms and three types of interstices occupied by D atoms in $Zr_2FeD_{3.39-5.00}$: Zr_4 (D1), Zr_3Fe (D2), Zr_4 (D3) and vacant interstice Zr_2Fe_2. Chains of Fe atoms perpendicular to paper plane, along [001]. (c) Crystal structure of $Zr_4Fe_2O_{0.6}$ (Fe_3W_3C type). Fe_4-tetrahedra and Zr_6-octahedra centred by O-atoms are shown.

Table 1
Crystallographic data for the Zr_3FeD_x ($x=1.27$; 2.54; 5.04; 6.70) deuterides

Compound	a, Å	b, Å	c, Å	V, Å^3	$\Delta a/a$, %	$\Delta b/b$, %	$\Delta c/c$, %	$\Delta V/V$, %	ΔV/at.D, Å^3
Zr_3Fe	3.324(2)	10.974(5)	8.821(3)	321.77(45)	–	–	–	–	–
$Zr_3FeD_{1.27}$	3.3261(4)	11.268(1)	8.999(1)	337.27(11)	0.06	2.68	2.02	4.8	3.05
$Zr_3FeD_{2.54}$	3.3536(4)	11.317(1)	9.200(1)	349.16(12)	0.89	3.13	4.30	8.5	2.70
$Zr_3FeD_{5.04}$	3.4524(1)	11.2333(5)	9.4846(4)	367.44(4)	3.86	2.36	7.55	14.2	2.27
$Zr_3FeD_{6.70}$	3.5803(3)	11.059(1)	9.6486(8)	382.03(9)	7.71	0.77	9.38	18.7	2.25

Table 2
Crystallographic data for the Zr_2FeD_x ($x=1.80$; 2.91; 3.39; 4.66; 5.00) deuterides

Compound	T, K	a, Å	c, Å	V, Å^3	$\Delta a/a$, %	$\Delta c/c$, %	$\Delta V/V$, %	ΔV/at.D, Å^3
Zr_2Fe	293	6.3787(9)	5.5988(6)	227.80(9)	–	–	–	–
$Zr_2FeD_{1.80}$	293	6.7301(4)	5.4298(4)	245.94(4)	5.51	−3.02	8.0	2.52
$Zr_2FeD_{2.91}$	293	6.8785(5)	5.5087(5)	260.64(6)	7.84	−1.61	14.4	2.82
$Zr_2FeD_{3.39}$	673	6.9213(9)	5.5657(10)	266.62(10)	8.51	−0.59	17.0	2.86
$Zr_2FeD_{4.66}$	473	6.959(1)	5.6222(9)	272.30(13)	9.10	0.42	19.5	2.39
$Zr_2FeD_{5.00}$	298	6.93566(8)	5.62061(8)	270.370(6)	8.73	0.39	18.7	2.13

Table 3
Selected crystal structure data for the Zr_3FeD_x ($x=1.27$; 2.54; 5.04; 6.70) deuterides derived from powder neutron diffraction experiments at 293 K

Compound	Interstices and their occupation, %				Mean Zr–D distances, Å			
	Zr_3Fe_2 (D1)	Zr_3Fe (D2)	$Zr_4(I)$ (D3)	$Zr_4(II)$ (D4)	Zr_3Fe_2 (D1)	Zr_3Fe (D2)	$Zr_4(I)$ (D3)	$Zr_4(II)$ (D4)
Zr_3Fe	–	–	–	–	2.053[c]	1.997[c]	2.026[c]	2.003[c]
$Zr_3FeD_{1.27}$[a]	–	–	–	63.5(15)	2.043[c]	2.034[c]	2.041[c]	2.064
$Zr_3FeD_{2.54}$[a]	–	–	47.5(24)	79.3(20)	2.029[c]	2.062[c]	2.062	2.099
$Zr_3FeD_{5.04}$[a]	36.0(13)	48.3(15)	91.9(11)	93.7(11)	2.103	2.105	2.082	2.113
$Zr_3FeD_{6.70}$[b]	91.1(10)	90.7(8)	92.9(8)	92.7(8)	2.159	2.098	2.103	2.132

[a] Reliability factors: $Zr_3FeD_{1.27}$: $R_p=0.059$; $R_{wp}=0.076$; $\chi^2=3.01$. $Zr_3FeD_{2.54}$: $R_p=0.059$; $R_{wp}=0.077$; $\chi^2=5.11$. $Zr_3FeD_{5.04}$: $R_p=0.044$; $R_{wp}=0.056$; $\chi^2=2.96$. Complete refinement results are published elsewhere [15].

[b] In the structure of saturated (1 bar D_2) $Zr_3FeD_{6.70}$ deuteride (space group *Cmcm*; No. 63) at 293 K atoms fill the following positions [7]: 4 Zr1 in 4*c*: 0; 0.4214(4); 1/4; $B_{iso}=0.74(8)$ Å^2; 8 Zr2 in 8*f*: 0; 0.1392(3); 0.0500(3); $B_{iso}=1.19(7)$ Å^2; 4 Fe in 4*c*: 0; 0.7161(3); 1/4; $B_{iso}=1.23(7)$ Å^2; D1 in 4*c*: 0; 0.2222(5); 1/4; $B_{iso}=1.49(6)$ Å^2; D2 in 8*f*: 0; 0.4094(3); 0.6458(4); $B_{iso}=1.66(8)$ Å^2; D3 in 8*f*: 0; 0.3275(3); 0.0558(4); $B_{iso}=1.66(8)$ Å^2; D4 in 8*f*: 0; 0.9622(4); 0.1288(3); $B_{iso}=1.69(9)$ Å^2.

[c] Empty interstices. Distances between the Zr atoms and the centre of the interstice are given.

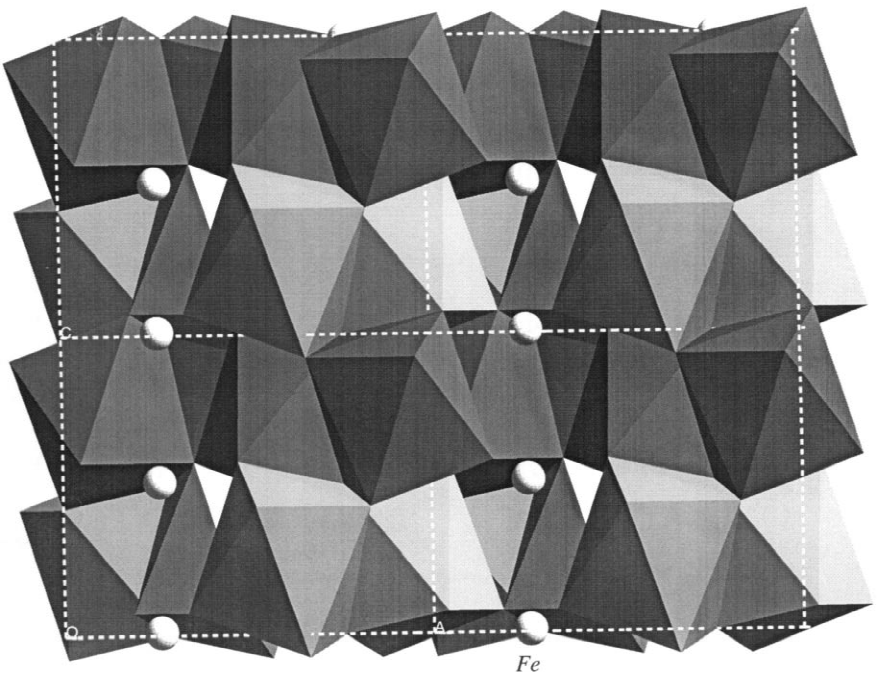

Fig. 2. Stacking of tetragonal antiprisms ZrD_8 in Zr_2FeD_5 viewed along [010].

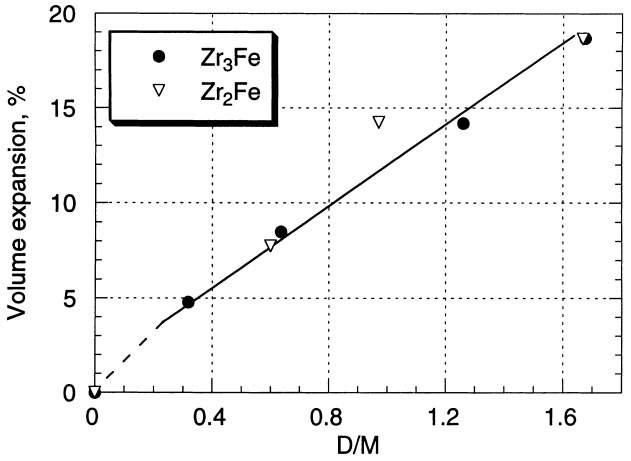

Fig. 3. Volume expansion vs deuterium content for Zr_2FeD_x and Zr_3FeD_x at 293 K.

structure of the intermetallic compounds and their corresponding hydrides, as derived from powder diffraction studies utilising conventional X-ray, synchrotron X-ray and neutron sources.

2. Experimental

The initial alloys were prepared from high purity zirconium (99.9%), iron (99.9) and iron oxide Fe_2O_3 (99.9%). Stoichiometric mixtures of these components were melted on a water-cooled copper pad in an argon arc furnace. Zr_2Fe was studied in the as cast state. The samples of Zr_3Fe and $Zr_4Fe_2O_{0.6}$ were respectively annealed at 1123 K (6 weeks) and 1273 K (4 weeks), before being quenched into ice water. Powder X-ray diffraction (PXD) data (Siemens D 5000 diffractometer; $CuK\alpha_1$ radiation, Bragg Brentano geometry, position sensitive detector) indicated the presence of nearly single phase materials. Trace amounts of impurities were found for the Zr_3Fe ($ZrFe_2$ and α-Zr) and Zr_2Fe ($ZrFe_2$, Zr_3Fe and α-Zr) samples. The derived unit cell parameters from PXD [Zr_3Fe: $a=3.324(2)$; $b=10.974(5)$; $c=8.821(3)$ Å), Zr_2Fe: $a=6.3787(9)$, $c=5.5988(6)$ Å and $Zr_4Fe_2O_{0.6}$: $a=12.180(1)$ Å] agreed well with literature data [11].

Deuterium gas (99.8% purity) was used in syntheses of the deuterides. The formation of the deuterides $Zr_3FeD_{6.7}$ and $Zr_2FeD_{5.0}$ and the $Zr_4Fe_2OH_{7.50}$ hydride was monitored by volumetric measurements. Deuterides with lower D-contents were obtained from the saturated $Zr_3FeD_{6.7}$ and $Zr_2FeD_{5.0}$ deuterides by application of secondary vacuum at selected desorption temperatures. The $Zr_3FeD_{5.04}$ and $Zr_2FeD_{2.91}$ deuterides were synthesised at 433 K, $Zr_3FeD_{2.54}$ and $Zr_2FeD_{1.80}$ at 573 K and $Zr_3FeD_{1.27}$ at 673 K.

Hydrogen absorption and desorption properties were studied by Temperature Pressure Analysis (TPA), Hydrogen Differential Thermal Analysis (HDTA) and Thermal Desorption Spectroscopy (TDS) techniques. Constant heating rates of 2 K/min (TDS) and 5 K/min (TPA and

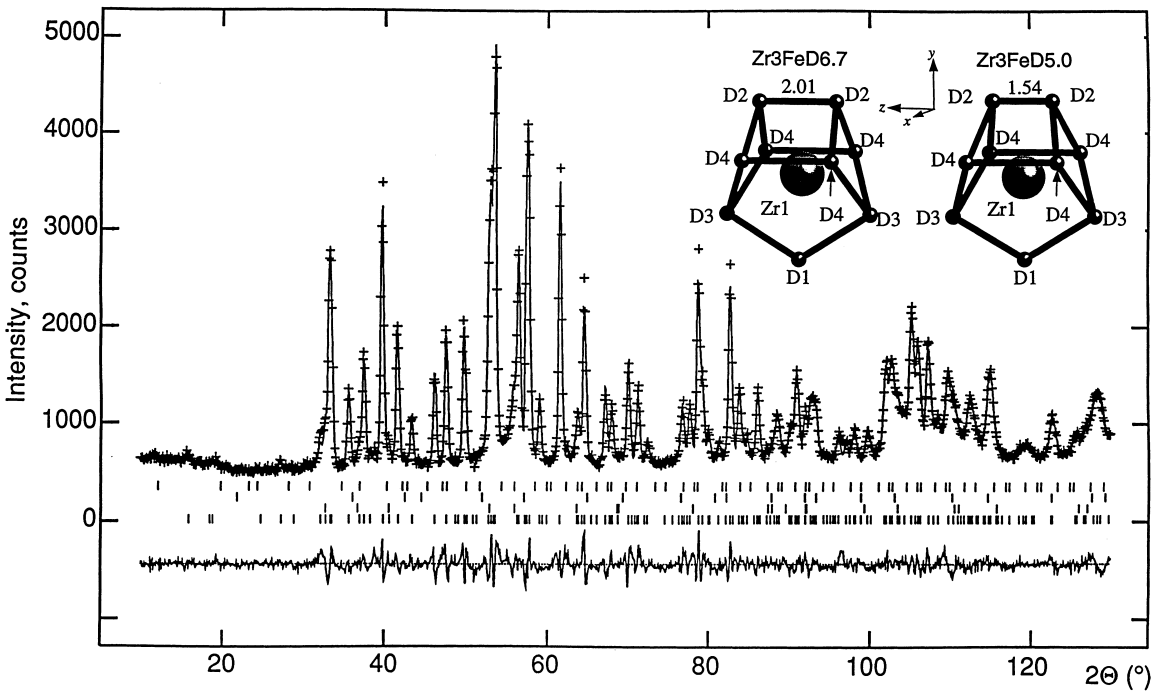

Fig. 4. Observed (+), calculated (upper line) and difference (lower line) powder neutron diffraction profile for $Zr_3FeD_{5.04}$ at 293 K. PUS instrument, $\lambda=1.5554$ Å. Positions of the peaks for the constituent phases are marked (from bottom to top): $Zr_3FeD_{5.04}$, ZrD_2, $ZrFe_2$, $Zr_4Fe_2OD_x$. [$Zr2D_9$] 9-vertexes polyhedra (inlet).

Table 4
Selected crystal structure data for the Zr_2FeD_x ($x=1.80$; 2.91; 3.39; 4.66; 5.00) deuterides derived from powder neutron diffraction experiments at 293, 298, 473 and 673 K

Compound	T, K	Space group	Interstices and their occupation, %				Mean Zr–D distances, Å		
			Zr_4 (4b; D1)	Zr_3Fe (D2)		Zr_4	Zr_4	Zr_3Fe	Zr_4
				16g	32m	(16l; D3)	(4b; D1)	(16g/32m; D2)	(16l; D3)
Zr_2Fe	–	*I*4/*mcm*	–	–	–	–	2.078[c]	1.965[c]	2.054[c]
$Zr_2FeD_{1.80}$[a]	293 K	*I*4/*mcm*	39.3(19)	–	3.3(8)	28.4(8)	2.096	2.030	2.093
$Zr_2FeD_{2.91}$[a]	293 K	*P*4/*ncc*	88.6(19)	50.8(8)	–	–	2.115	2.053	2.128[c]
$Zr_2FeD_{3.39}$[a]	673 K	*I*4/*mcm*	60.0(10)	–	26.0(5)	17.7(6)	2.134	2.077	2.145
$Zr_2FeD_{4.66}$[a]	473 K	*P*4/*ncc*	100	91.6(6)	–	–	2.132	2.095	2.156[c]
$Zr_2FeD_{5.00}$[b]	298 K	*P*4/*ncc*	100	100	–	–	2.117	2.091	2.149[c]

[a] Reliability factors: $Zr_2FeD_{1.80}$: $R_p=0.050$; $R_{wp}=0.065$; $\chi^2=1.48$. $Zr_2FeD_{2.91}$: $R_p=0.051$; $R_{wp}=0.066$; $\chi^2=1.38$. $Zr_2FeD_{3.39}$: $R_p=0.033$; $R_{wp}=0.045$; $\chi^2=8.94$. $Zr_2FeD_{4.66}$: $R_p=0.032$; $R_{wp}=0.043$; $\chi^2=9.03$. Complete refinement results will be published elsewhere [16,17].

[b] In the structure of saturated (1 bar D_2) Zr_2FeD_5 deuteride (space group *P*4/*ncc*; No. 130) at 298 K atoms fill the following positions [3]: 8 Zr in 8*f*: 0.4114(2); 0.5886(2); 1/4; $B_{iso}=0.80(2)$ Å^2; 4 Fe in 4*c*: 1/4; 1/4'; 0.0109(3); $B_{iso}=1.10(4)$ Å^2; D1 in 4*b*: 3/4; 1/4; 0; $B_{iso}=1.95(3)$ Å^2; D2 in 16*g*: 0.0320(2); 0.1657(2); 0.0760(2); $B_{iso}=1.95(3)$ Å^2.

[c] Empty interstices. Distances between the Zr atoms and the centre of the interstice are given.

HDTA) were used. The alloys and the hydrogenated intermetallics were studied by standard SEM (JEOL 6300) and by high resolution SEM (HRSEM-Hitachi S-4000 FE).

Synchrotron (SR) PXD data were collected at the Swiss–Norwegian Beam Line, BM1, at ESRF, Grenoble, using monochromatic X-rays ($\lambda=0.65015$ Å) obtained from Si(111). The $Zr_2FeD_{2.9}$ sample was kept in a rotating 0.3 mm sealed glass capillary and was heated by means of a heat-blower. Diffraction data were collected at 293, 353, 408, 453, 503, 548 and 568 K.

Powder neutron diffraction (PND) data were collected with the PUS instrument ($\lambda=1.5554$ Å; $2\Theta=10$–$130°$; $\Delta 2\Theta=0.05°$; $T=293$ K) at Institute for Energy Technology, Kjeller, Norway and at Studsvik Neutron Research Laboratory ($\lambda=1.116$ Å; $2\Theta=3.8$–$137°$; $\Delta 2\Theta=0.1°$; $T=293$ K; 473 K; 673 K; 873 K; 1073 K), Sweden. The samples were contained in a sealed, cylindrical vanadium holder with 5 mm inner diameter (Kjeller) or, for the in situ studies at Studsvik, inside a quartz tube under a deuterium pressure of 1 bar. The GSAS (General Structure Analysis System) software [12] was used in the Rietveld type profile refinements. Nuclear scattering lengths $b_{Zr}=7.16$, $b_{Fe}=9.50$ and $b_D=6.67$ fm were taken from Ref. [13].

3. Results and discussion

3.1. Zr–Fe intermetallics as possible hydrogen absorbers

The architecture of the crystal structures of Zr_3Fe

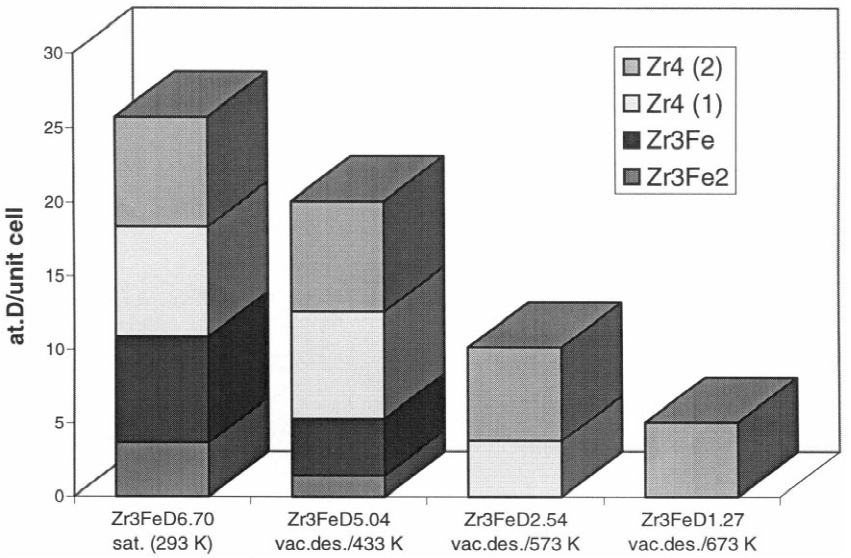

Fig. 5. Site occupancy for D-atoms in interstices of Zr_3FeD_x.

(orthorhombic; Re_3B-type), Zr_2Fe (tetragonal; $CuAl_2$-type) and $Zr_4Fe_2O_{0.6}$ (cubic; Fe_3W_3C-type) differ in many respects. In all these zirconium-rich phases, Zr atoms form the major part of the structure skeleton and its building units (Fig. 1(a–c)). The skeletons are composed of different units: Fe-centred trigonal prisms Zr_6 (Zr_3Fe), tetragonal antiprisms Zr_8 (Zr_2Fe) and octahedra Zr_6, both normal and O-centred ($Zr_4Fe_2O_{0.6}$). All these compounds contain a number of Zr-rich interstices suitable for hydrogen absorption. On the other hand, the Fe–Fe bonding is significantly different. Separate Fe_4 tetrahedra exist in $Zr_4Fe_2O_{0.6}$ (Fig. 1(c)), whereas chains of Fe atoms are found in Zr_2Fe (Fig. 1(b)). In Zr_3Fe (Fig. 1(a)) no direct Fe–Fe bonds are present, and consistent with this fact, the only Fe-containing tetrahedral interstices are Zr_3Fe tetrahedra. The other compounds, Zr_2Fe and $Zr_4Fe_2O_{0.6}$, contain interstices with more than 25 at% Fe.

3.2. Hydrogen ordering in Zr_2Fe- and Zr_3Fe-based hydrides; saturated deuterides

The metal sublattices of Re_3B- and $CuAl_2$-types for Zr_3Fe and Zr_2Fe, respectively, are preserved on hydrogenation. In both cases, the formation of the saturated

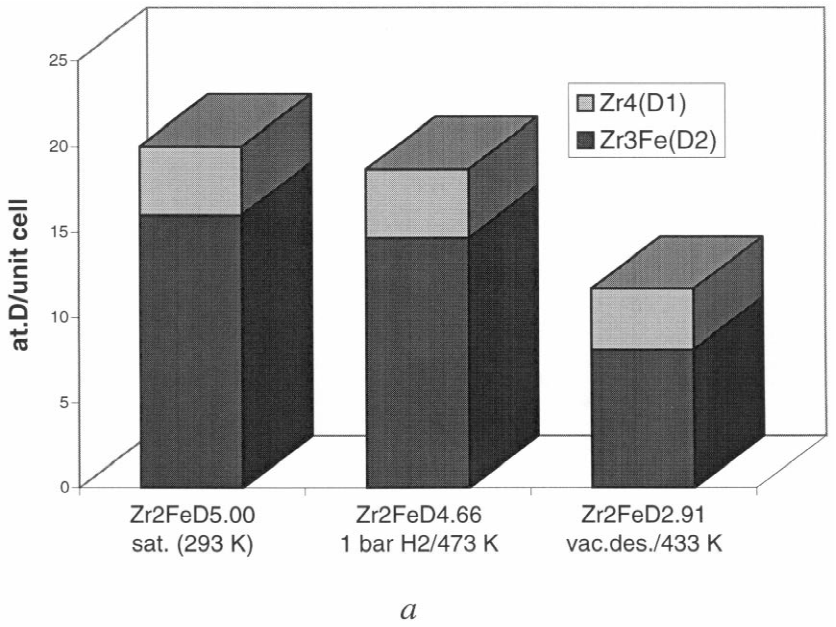

a

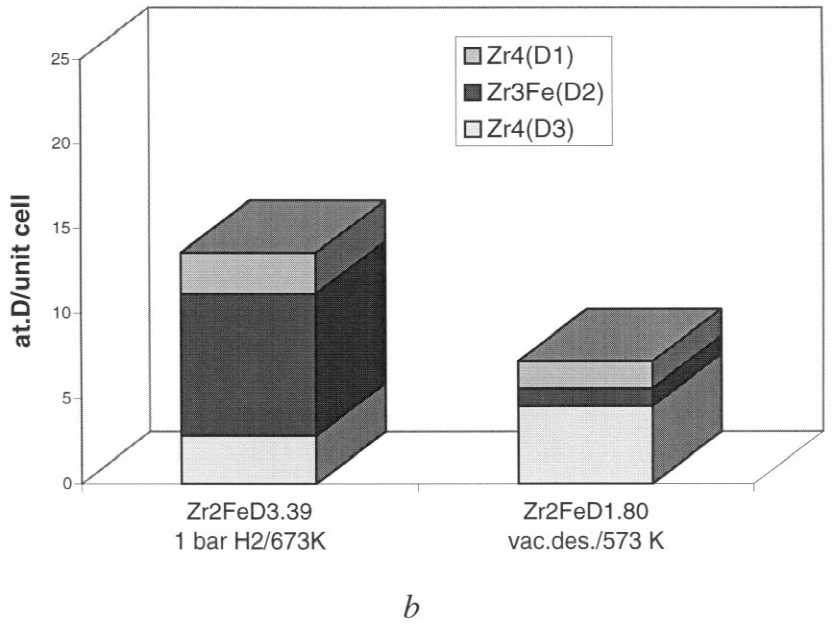

b

Fig. 6. Site occupancy for D-atoms in interstices of Zr_2FeD_x; samples with (a) ordered hydrogen sublattice (space group $P4/ncc$); (b) disordered hydrogen sublattice (space group $I4/mcm$).

deuterides with a D/(Zr+Fe) ratio of 1.67, i.e., $Zr_3FeD_{6.7}$ [7] and $Zr_2FeD_{5.0}$ [3], are accompanied by an anisotropic volume expansion of 18.7%. The main expansion occurs in the *ac*-plane for the orthorhombic $Zr_3FeD_{6.70}$ (Table 1) and in the *ab*-plane for the tetragonal $Zr_2FeD_{5.0}$ (Table 2), with additional, rather small elongations of *b* and *c*, respectively.

In Zr_3Fe there are 10 crystallographically different interstices (76 interstices/unit cell; $Z=4$) including eight types of tetrahedra [five types Zr_3Fe (48/unit cell; $r=$ 0.40–0.53 Å); three types Zr_4 (20/unit cell; $r=0.50$–0.62 Å)], a trigonal bipyramid Zr_3Fe_2 (4/unit cell; $r=0.52$ Å) and one octahedron Zr_6 (4/unit cell; $r=0.80$ Å). $Zr_3FeD_{6.7}$ exhibits an ordered structure with nearly complete deuterium filling of four different types of interstices (see Fig. 1(a)), one Zr_3Fe_2-, one Zr_3Fe- and two Zr_4-interstices. The occupied intertices have radii filling a narrow range 0.49–0.53 Å. When being outside that range, they become empty. The main part of the occupied interstices, i.e., 16 out of 28 per unit cell, are formed solely by zirconium atoms.

One point concerning the deuterium distribution in $Zr_3FeD_{6.7}$ should be noted in addition. An alternative way of filling the interstices, which would allow a maximal D/(Zr+Fe) ratio of eight is not realised. In that model (24 D in Zr_3Fe- and 8 D in Zr_4-tetrahedra) 75% of the relevant interstices include Fe in their surroundings. This is apparently a less favourable bonding situation for the H(D) atoms than the observed model with hydrogen mainly situated in Zr_4-tetrahedra [7].

For Zr_2Fe the unit cell contains 68 tetrahedral interstices of four non-equivalent types; two types Zr_4 tetrahedra (4 and 16/unit cell), one Zr_3Fe tetrahedron (32/unit cell) and one Zr_2Fe_2 tetrahedron (16/unit cell;). In $Zr_2FeD_{5.0}$ two of these tetrahedral interstices [Zr_3Fe ($r=0.48$ Å) and Zr_4 ($r=0.52$ Å)] are occupied by deuterium atoms in an ordered way. Note that the majority of filled sites contain Fe-surrounding atoms (16 out of 20 filled interstices) and that an alternative, possible model for site-filling in Zr_2FeD_5, with D-atoms in Zr_4-tetrahedra (16/unit cell; $r=0.55$ Å) and in 25% of the Zr_2Fe_2 tetrahedra (4/unit cell; $r=0.38$ Å), is not realised. Again, as in case of $Zr_3FeD_{6.70}$, it should be noted that the occupied interstices have similar radii range of 0.48–0.52 Å.

3.3. Hydrogen sublattice

In the crystal structures for $Zr_2FeD_{5.0}$ and $Zr_3FeD_{6.7}$ the coordination polyhedra for the occupied interstices share common edges and vertices. All D–D separations fulfil the so-called ''rule of 2 Å'' [14] [shortest D–D distances are 2.01 ($Zr_3FeD_{6.7}$ [7]) and 2.08 Å ($Zr_2FeD_{5.0}$ [3])]. In both cases the hydrogen sublattices can be presented as built from polyhedra formed by deuterium atoms surrounding Zr-atoms. In $Zr_3FeD_{6.7}$ the D-sublattice consists of deformed cubes (ZrD_8) and deformed cubes with an additional ninth vertex (ZrD_9). In $Zr_2FeD_{5.0}$ the coordination polyhedron is a tetragonal antiprism (ZrD_8). For both structure types these polyhedra form a spatial framework by sharing vertices and edges (see Fig. 2 where the D-sublattice in $Zr_2FeD_{5.0}$ is given as an example).

3.4. Lower deuterides

Over the whole range of D-contents $0<D/Me<1.67$ PXD studies of the Zr_3Fe–D_2 and Zr_2Fe–D_2 systems show that deuterides, $Zr_3FeD_{1.27-6.70}$ and $Zr_2FeD_{1.80-5.00}$, are formed with the metal matrix retaining the original Re_3B and $CuAl_2$ structure types.

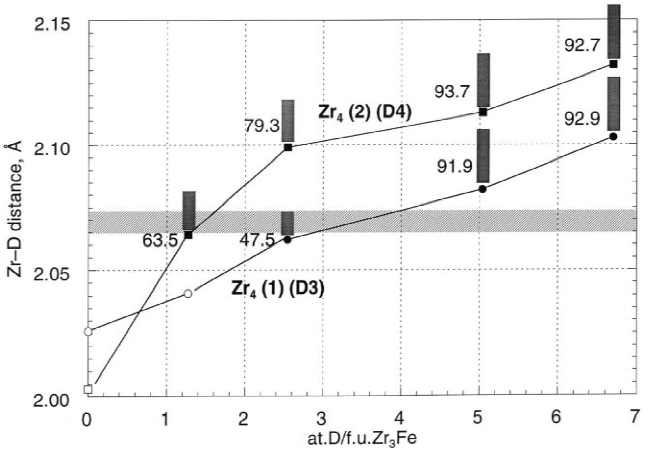

Fig. 7. Zr–D distances in occupied (●, ■) and vacant (○, □) Zr_4-tetrahedra of Zr_3FeD_x. Heights of bars represent site occupancy. The range for Zr–D bonds in ZrD_2 is shaded.

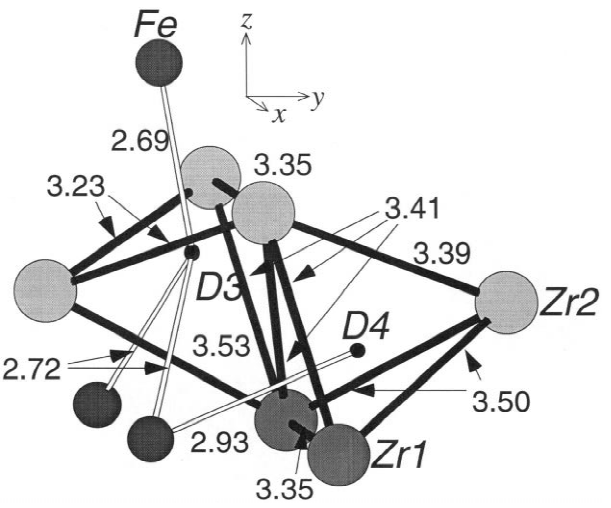

Fig. 8. Part of the crystal structure for $Zr_3FeD_{2.54}$. Zr–Zr bonds in the Zr_4-tetrahedra and D–Fe distances for the D3 and D4 interstices are shown.

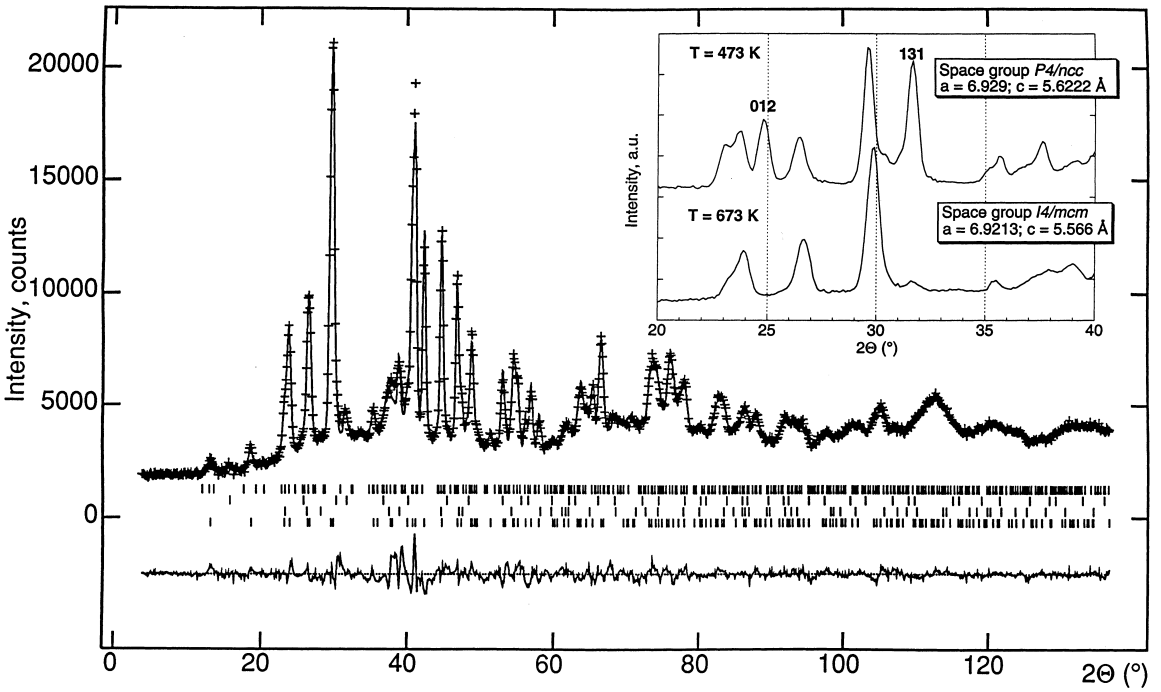

Fig. 9. Observed (+), calculated (upper line) and difference (lower line) powder neutron diffraction profile for $Zr_2FeD_{3.39}$ at 673 K (in situ measurements under 1 bar D_2). Wavelength $\lambda = 1.116$ Å. Positions of the peaks for the constituent phases are marked (from bottom to top): $Zr_2FeD_{3.39}$, ZrD_2, $ZrFe_2$, $Zr_3FeD_{6.7}$. Temperature evolution of the diffraction pattern ($2\Theta = 20–40°$) on heating from 473 to 673 K is shown in insert; Miller indices for superstructure peaks given.

The unit cell volumes gradually increase with increasing deuterium contents in the metal lattice of Zr_3Fe and Zr_2Fe (Tables 1,2; Fig. 3). The volume increment on introduction of deuterium is composition dependent. The smallest volume increment per absorbed D-atom is found for the saturated deuterides $Zr_2Fe_{5.00}$ and $Zr_3FeD_{6.7}$; 2.13–2.25 $Å^3$/D. At low D-contents the increment is larger, reaching 3.05 $Å^3$/D for $Zr_3FeD_{1.27}$.

The unit cell expansion on deuteration is anisotropic in the $Zr_2Fe–D_2$ and $Zr_3Fe–D_2$ systems. For Zr_3FeD_x there

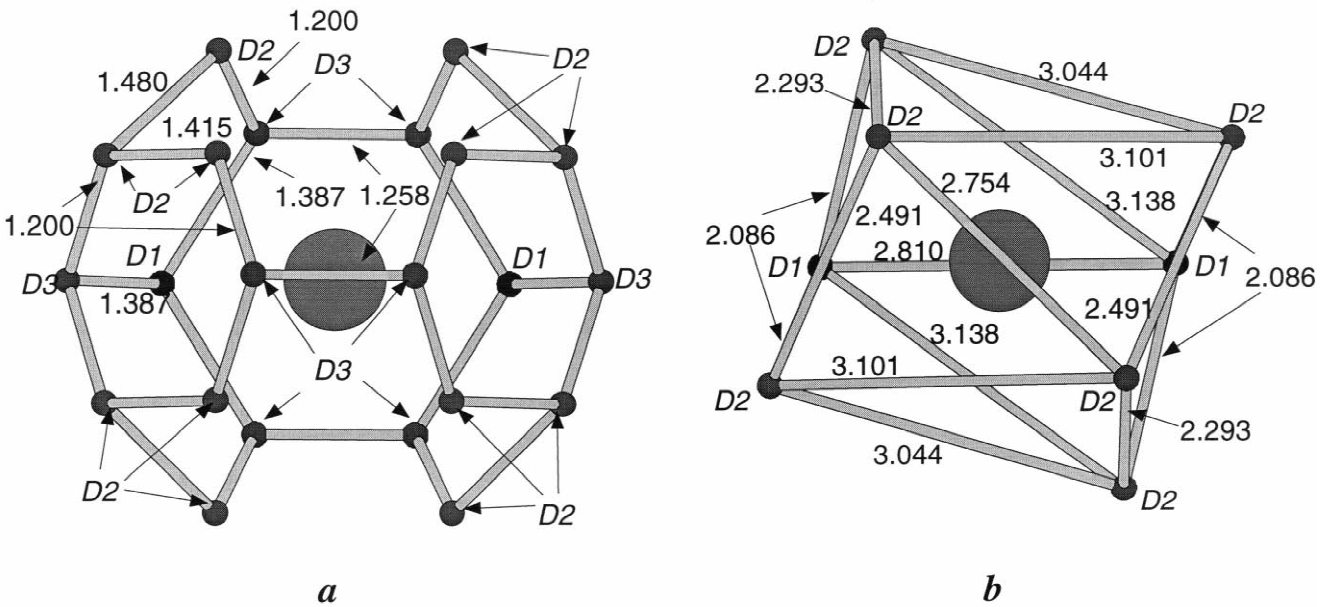

Fig. 10. Coordination of Zr-atom by D-sites in (a) disordered structure of $Zr_2FeD_{1.80}$ (space group $I4/mcm$) and (b) ordered structure of $Zr_2FeD_{5.0}$ (space group $P4/ncc$).

is a gradual, continuous expansion in [100] and [001] with increasing D-content. The variation in $\Delta b/b$ (see Table 1) is unsystematic, and actually the saturated deuteride has the smallest $\Delta b/b$ shift relative to the initial alloy. For Zr_2FeD_x the expansion of the tetragonal unit cell proceeds exclusively in the *ab*-plane and is accompanied by a shrinkage of the *c*-axis, most notably for the lowest deuteride studied, i.e., $Zr_2FeD_{1.80}$, see Table 2.

The anisotropic expansion can be related to preferred occupation of hydrogen atoms in certain interstices and to repulsive D–D interactions. One example is the transformation $Zr_3FeD_{5.04} \rightarrow Zr_3FeD_{6.70}$ (Fig. 4). In $Zr_3FeD_{5.04}$, the Zr_3Fe interstices (D2-sites) have a partial occupancy of around 50%, which in average allows a short distance between the sites (1.54 Å). However, in the saturated deuteride these sites are almost completely occupied. This requires a considerably longer D2–D2 distance (2.01 Å) in order to fulfil the ''rule of 2 Å'' [14]. The anisotropic unit cell expansion can therefore be related to D2-D2 repulsion along [001] (see Table 1).

Similar arguments hold for the anisotropic expansion of the tetragonal unit cell of $Zr_2FeD_{5.00}$. The shortest D–D distances (2.08 Å) are located within the *ab*-plane and the expansion on deuteration occurs mainly within this plane. However, the anisotropy is already considerable at low D-contents. In these, a major part of the D-sites separated by the shortest D–D distances (Table 4) are empty, and a more complex explanation involving local D–D repulsions is probably needed.

3.5. H/D site preferences

On decreasing D-content, the deuterium is preferentially withdrawn from Fe-containing interstices, as evident from Figs. 5,6 and Tables 3,4. In that respect one may consider the D-atoms occupying Zr_3Fe_2-trigonal bipyramids (Zr_3FeD_x) and the Zr_3Fe-tetrahedra (Zr_3FeD_x and Zr_2FeD_x) to be weaker bonded to the metal matrix. The two types of Zr_4-tetrahedra in Zr_3FeD_x remain nearly completely occupied for $D/M > 0.60–0.65$. For lower D/M ratios, the two Zr_4-sites start to become differently occupied and for $Zr_3FeD_{2.54}$ the Zr_4(I)-site (D3) has 48% occupancy compared to 79% for D4 in the Zr_4(II)-site. In the lowest studied deuteride, $Zr_3FeD_{1.80}$, only the Zr_4(II)-site is partially occupied (64%). In general, a reduced occupancy of a certain site appears to correlate with shortening of the Zr/Fe–D bond distances. The reduced occupancy of the Zr_4(I)-site (D3) correlates with (a) shorter D3–Zr bond distances compared to that of the more completely filled D4 position (Fig. 7); (b) slightly shorter Zr–Zr distances in the surrounding Zr_4-tetrahedron (Fig. 8); (c) short separations from the Zr_4(I)-interstice to the next nearest Fe neighbouring atoms (three distances at 2.69–2.72 Å) in contrast to one Fe neighbour for the occupied Zr_4(II)-interstice (D4) at a distance of 2.93 Å (Fig. 8).

For Zr_2FeD_x, deuterium is mainly released from the Zr_3Fe-interstices (Fig. 6). For the lowest deuteride studied here, $Zr_2FeD_{1.80}$, the D-sublattice is no longer ordered. Instead a change in space group symmetry occurs (from *P*4/*ncc* to *I*4/*mcm*) implying distribution of D-atoms over three types of interstices (Fig. 6(b)).

The observed Zr–D bond lengths for the occupied Zr_4-tetrahedra in Zr_3FeD_x and Zr_2FeD_x correspond well to those of similar Zr_4-tetrahedra in binary zirconium deuterides. In intermetallic deuterides these tetrahedra become filled up with D-atoms until the Zr–D distances exceed those in ZrD_2 (see Tables 3,4). When the contraction of the Zr_4-tetrahedra proceeds for the lower deuterides and the Zr–D distances become shorter than those charac-

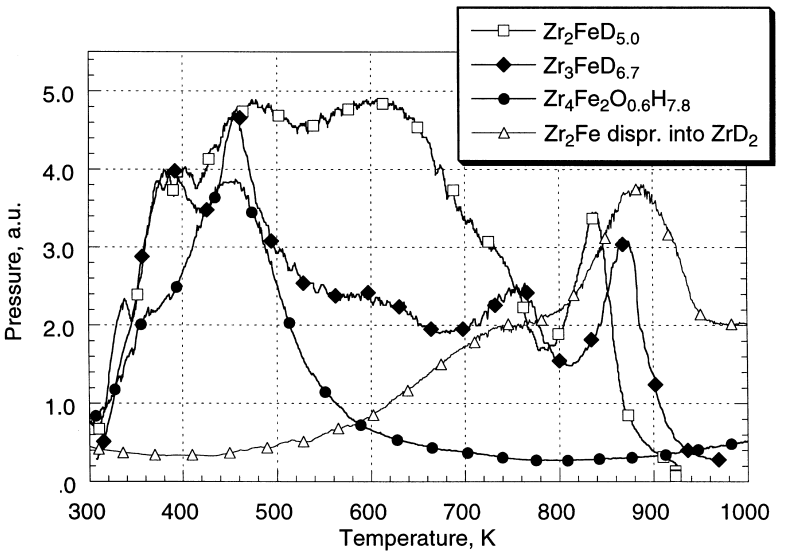

Fig. 11. Hydrogen desorption traces for Zr–Fe-based hydrides.

teristic for ZrD_{2-x} (2.065–2.073 Å), the Zr–D bonding appears to become unstable, and complete D-desorption proceeds from at temperatures significantly lower than for ZrD_2.

3.6. Order–disorder transition for Zr_2FeD_{5-x}

During in situ PND studies, the saturated $Zr_2FeD_{5.00}$ deuteride was heated under 1 bar D_2 gas pressure from 293 to 1073 K in steps of 200 K. At 473 K the hydrogen sublattice corresponds to the tetragonal structure observed for $Zr_2FeD_{5.00}$ (space group $P4/ncc$) at 298 and 4.2 K [3]. A partial deuterium desorption, reducing the D/M ratio from 5.00 to 4.66, is limited to a small D-release from the Zr_3Fe-interstices, whereas the Zr_4-sites remain completely occupied. There is no significant change in the relative amounts of the three minor impurity phases ($ZrFe_2$, ZrD_2 and $Zr_3FeD_{6.70}$) on heating from 293 to 473 K. This clearly shows that no disproportionation of Zr_2FeD_{5-x} takes place at modest operating temperatures.

On heating further up to 673 K, a more considerable deuterium desorption takes place. For the material with refined composition $Zr_2FeD_{3.39}$ an order–disorder transition has obviously occurred. The transition implies an increased symmetry from space group $P4/ncc$ to $I4/mcm$ (the latter corresponds to that of Zr_2Fe) as evidenced by the disappearance of a few strong PND reflections (see Fig. 9). In the ''low temperature'' structure ($P4/ncc$) two interstices, Zr_4 and Zr_3Fe, are filled by D atoms in an ordered way. At and above 673 K, the D-atoms in Zr_3Fe-interstices are distributed over 32 sites/unit cell, whereas at 473 K one subgroup of 16 sites is filled, another is completely empty.

In the disordered model, Zr is surrounded by 22 D-sites (see Fig. 10(a)) with neighbour–neighbour distances less than 1.4 Å. In the saturated deuteride, only eight of these 22 sites are occupied, and the deformed tetragonal antiprismatic coordination polyhedron (Fig. 10(b)) provides D–D separations above 2.085 Å.

3.7. Hydrogen absorption–desorption properties

The successful deuteration of Zr_2Fe at very mild conditions, i.e., at room temperature, $p(D_2)<0.25$ bar and without preliminary activation, confirms its excellent H-getter properties. Also for Zr_3Fe, absorption of deuterium is possible at room temperature and $p(D_2)<1$ bar, however, a preliminary activation is required. In contrast, hydrogenation of the oxygen-containing intermetallic, $Zr_4Fe_2O_{0.6}$, is significantly different. $Zr_4Fe_2O_{0.6}$ has to be heated up to 620–670 K (1 bar H_2) to initiate hydrogen absorption, which results in an interstitial type hydride $Zr_4Fe_2O_{0.6}H_{7.80}$ with expanded cubic unit cell ($\Delta V/V=$ 17.8%).

Under secondary vacuum conditions, hydrogen desorption proceeds continuously over a wide temperature range for both the $Zr_2FeD_{5.00}$ and $Zr_3FeD_{6.70}$ deuterides. The desorption is completed at 923 K (Fig. 11). For Zr_3FeD_x one then observes a reversible formation of the initial intermetallic compound.

The $CuAl_2$-type metal lattice of Zr_2Fe seems to become substantially stabilised subsequent on hydrogen absorption. Note that the Zr_2Fe intermetallic itself exists in the narrow temperature range of 1048–1247 K [18]. No signs of disproportionation were seen by in situ PXD (SR) studies of $Zr_2FeD_{2.91}$ at 560 K (Fig. 12). However, the high resolution diffractograms clearly revealed that the initial normal thermal expansion was followed by decreased unit cell dimensions owing to deuterium desorption, before one

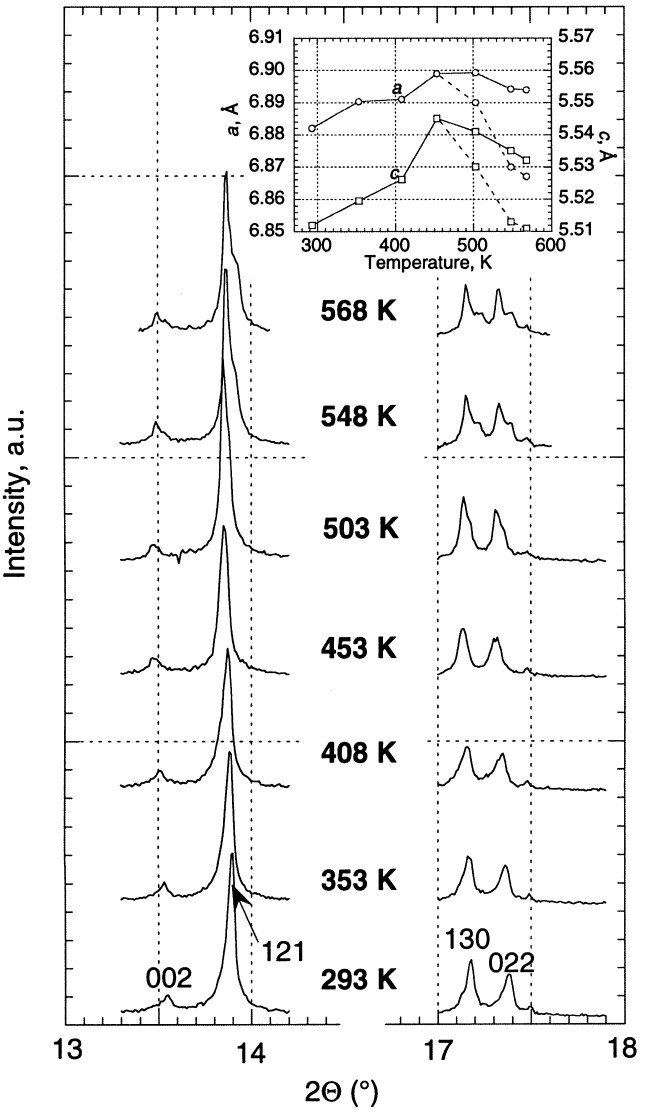

Fig. 12. Temperature evolution of selected part of powder X-ray diffraction (SR) pattern ($\lambda=0.65015$ Å; Miller indices given) of the $Zr_2FeD_{2.91}$ deuteride (293–568 K) together with corresponding changes in unit cell parameters (insert).

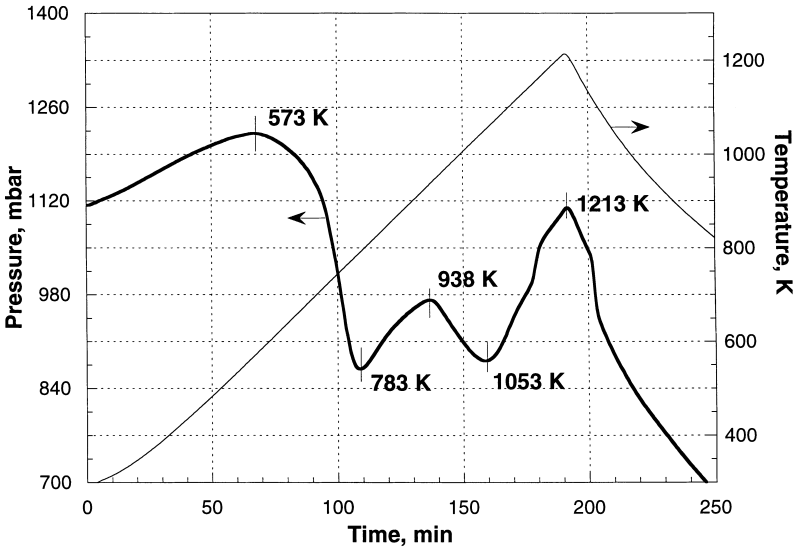

Fig. 13. Temperature–pressure analysis trace for $Zr_4Fe_2O_{0.6}$ heated in H_2 up to 1213 K.

at 503 K observed the formation of a two-phase mixture of closely related deuterides with different D/M contents.

After deuterium absorption, it is possible for Zr_2FeD_x to undertake a reversible absorption–desorption cycle. The $CuAl_2$-type metal sublattice is retained up to about 783 K, i.e., 265 K below the lower temperature stability limit for Zr_2Fe [18]. At 783 K the unit cell dimensions (a = 6.373(2); c = 5.579(2) Å; measured for cooled sample at 298 K) corresponds to those characteristic for the initial Zr_2Fe intermetallic (a = 6.3787(9), c = 5.5988(6) Å), indicating complete D-desorption. PXD shows increased amounts of the admixtural phase constituents, Zr_3Fe and $ZrFe_2$, indicating a partial disproportionation according to the scheme:

$$4\,Zr_2FeD_x + (1-2x)\,D_2 \rightarrow 2\,Zr_3Fe + ZrFe_2 + ZrD_2$$

Oxygen insertion into the metal matrix of Zr_2Fe significantly decreases both hydrogen absorption capacity (down to 1.3 H/M) and the thermal stability of the corresponding hydrides. For $Zr_4Fe_2O_{0.6}H_{7.80}$ hydrogen desorption is already complete at 573 K, with a distinct peak at 488 K (Fig. 11). The lower stability of $Zr_4Fe_2O_{0.6}H_{7.80}$ can be associated with the fact that Zr_4-tetrahedra are absent and that the hydrogen atoms therefore only can enter Fe-containing interstices.

3.8. The hydrogenation–disproportionation–desorption–recombination process

In addition to the formation of interstitial type hydrides described above, the studied compounds undergo two more

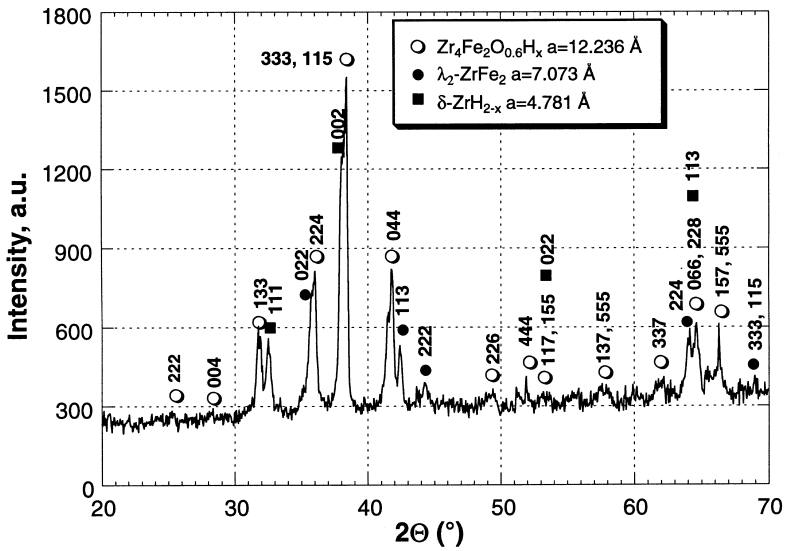

Fig. 14. X-ray diffraction pattern of $Zr_4Fe_2O_{0.6}$ after heating in H_2 up to 1213 K.

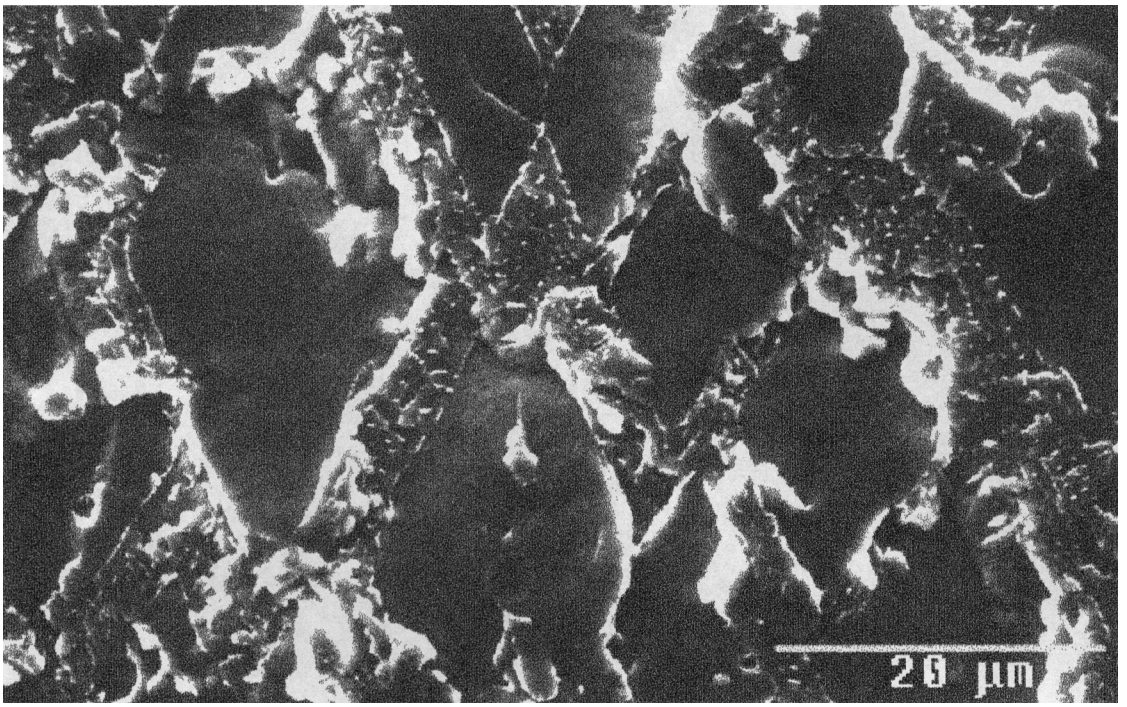

Fig. 15. Secondary HRSEM image of Zr_2Fe-alloy after HDDR processing at 923 K. Large rhombohedral grains Zr_3Fe, intergranular eutectic $ZrFe_2$ and α-Zr.

transformations during heating in hydrogen gas up to 1213 K;

(i) a partial hydrogen desorption followed by H-absorption and disproportionation of the metal matrix (see Fig. 13 as an example) and;
(ii) polymorphic transformation between tetragonal ε-ZrD_{2-x} and f.c.c. δ-ZrD_{2-x} in connection with a smaller H-desorption.

According to PXD, complete disproportionation occurs for Zr_3Fe:

$$2\,Zr_3Fe + (5 - 5x/2)\,H_2 \rightarrow 5\,ZrH_{2-x} + \lambda_2 - ZrFe_2$$

Similarly, in situ PND studies of Zr_2FeD_x show that a disproportionation takes place between 673 and 873 K:

$$2\,Zr_2FeD_{2.80} \rightarrow 3\,\varepsilon\text{-}ZrD_{1.87}\,(\text{tetragonal}) + \lambda_2 - ZrFe_2$$

On further heating to 1073 K (under 1 bar D_2 pressure),

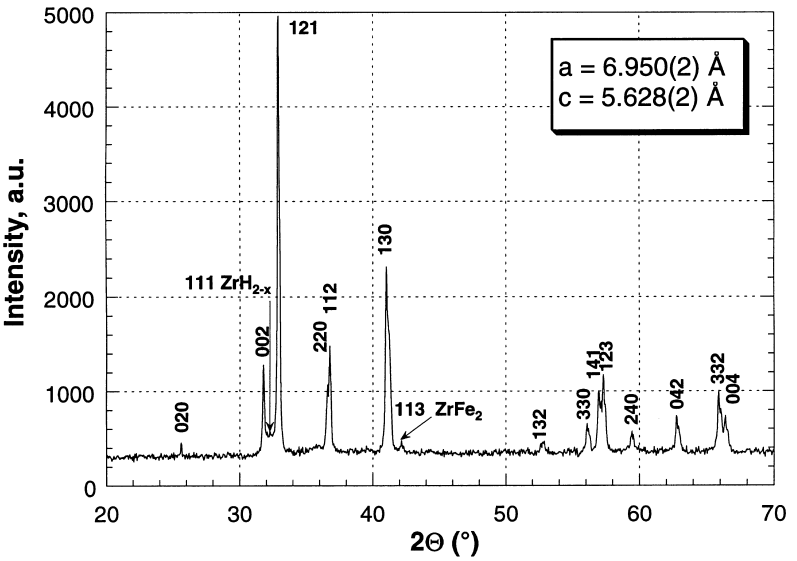

Fig. 16. X-ray diffraction pattern of Zr_2FeH_{5-x} synthesised from recombined alloy. Minor traces of ZrH_{2-x} and $ZrFe_2$ originate from inhomogeneity of the initial alloy.

ε-ZrD_{2-x} partially looses deuterium. The D/Zr ratio is reduced from 0.933 for ε-ZrD_{2-x} at 873 K to 0.75 for the formed cubic δ-ZrD_{2-x} at 1073 K.

Under the same conditions, the η-oxide $Zr_4Fe_2O_{0.6}$ also undergoes a partial disproportionation, with onset at 940 K. According to PXD, this results in formation of $ZrFe_2$ and $ZrO_{1-x}H_y$ (Figs. 13, 14). The disproportionation is rather slow and was not completed during the experiment (heating in hydrogen gas [P_{H_2}~1 bar] from room temperature up to 1213 K at a rate of 5 K/min.

All the disproportionated materials (originally being Zr_3FeD_{6-x}, Zr_2FeD_{4-x} and $Zr_4Fe_2O_{0.6}H_x$) desorb hydrogen around 873–893 K. This temperature corresponds exactly to the decomposition temperature of ZrD_2 (see Fig. 11). This hydrogen desorption is accompanied by a complete recombination of the intermetallic phases, i.e., Zr_2Fe, Zr_3Fe and $Zr_4Fe_2O_{0.6}H_x$, as indicated by PXD.

Zr_2Fe exists over a limited temperature range, and hence the scheme for recombination depends on the temperature range used for the hydrogen desorption. At 873–923 K, Zr_3Fe will be formed instead of Zr_2Fe. Considering the nominal composition of the material, the recombined alloy must also contain α-Zr formed by reaction between ZrD_{2-x} and $ZrFe_2$ formed in the initial stage of the disproportionation. This was confirmed both by PXD studies and by examination of the microstructure (Fig. 15). However, heating the recombined sample to 1073 K, which is within the stability region of Zr_2Fe [18], gives complete recombination into Zr_2Fe. This is evident from the PXD data in Fig. 16 for Zr_2FeH_{5-x} being synthesised under mild condition from a recombined material subjected to several full HDDR cycles. With basis in the present phase-structural transformations, a tentative phase diagram for the Zr_2Fe–D_2 system is proposed in Fig. 17.

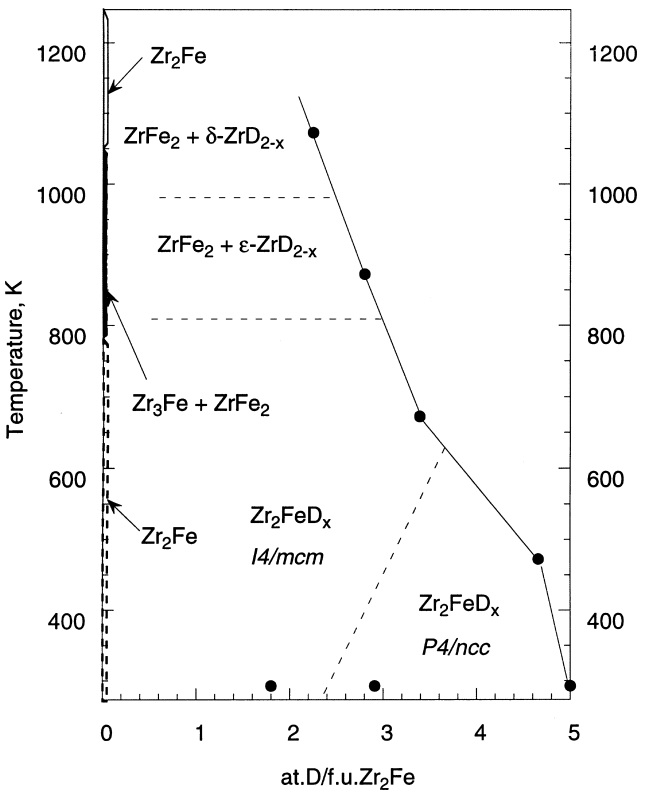

Fig. 17. Tentative phase diagram for Zr_2Fe–D_2.

4. Conclusions

The interplay between metal–metal, metal–hydrogen and hydrogen–hydrogen interactions determine the structural behaviour of hydrogenated Zr–Fe intermetallics. Hydrogen incorporation appears to increase the thermodynamic stability of the original metal matrices. This also concerns disproportionation into binary zirconium hydride. Reversible hydrogen absorption–desorption cycling is possible in these systems of the type ''intermetallic compound — insertion type hydride''. The hydrogen sublattices in the saturated deuterides, $Zr_3FeD_{6.70}$ and $Zr_2FeD_{5.00}$, are governed by the ''rule of 2 Å'', with deuterium forming 8- or 9-vertex polyhedra around the Zr-atoms. Shorter D–D distances, 1.4–1.5 Å, are calculated for the lower deuterides. However, these are associated with a partial site occupancy, e.g., subsequent on the order–disorder transition (Zr_2Fe–D_2 system). For the intermetallic Zr_3Fe-based hydrides, the distances from Zr to the centre of Zr_4-tetrahedral interstices, either occupied or vacant, correspond to the Zr–D bond lengths in binary zirconium hydride. The occupied interstices in the structures of saturated deuterides $Zr_3FeD_{6.70}$ and $Zr_2FeD_{5.00}$ have radii filling a narrow range $0.48 \leq r_i \leq 0.53$ Å.

The presence of oxygen influences significantly the H-storage behaviour of the Zr–Fe alloys. Both the storage capacity and the thermal stability is reduced for $Zr_4Fe_2O_{0.6}H_x$. However, for the first time the HDDR process was successfully applied to an oxygen-containing compound. The process is accompanied by transfer of O-atoms between Zr-oxyhydride and $Zr_4Fe_2O_{0.6}$. The universality of the HDDR process for the alloys of Zr and Fe is confirmed by the studies of the binary intermetallics, Zr_3Fe and Zr_2Fe.

Acknowledgements

Financial support from the Research Council of Norway and from Hydro Megon is gratefully acknowledged. Dr. R. McGreevy, Dr. R. Delaplane (Studsvik Neutron Research Laboratory, Uppsala University) and Dr. O. Gutfleisch (Birmingham University) are sincerely thanked for the in situ measurements of neutron diffraction data for the Zr_2Fe-based deuterides (RMcG and RD) and for the microstructural characterisation of the studied materials (OG). The opportunity to collect the data at the Swiss–

Norwegian Beamline, ESRF is sincerely appreciated. We thank Dr. K. Schenk (Universite de Lausanne) for lending us the heat-blower).

References

[1] P. Raj, P. Suryanarayana, A. Satnyamoothy, H. Shashikale, R.M. Iyer, J. Alloys Compds. 178 (1992) 393.
[2] A. Nobile, W.C. Mosley, J.C. Holder, K.N. Brooks, J. Alloys Compds. 206 (1994) 83.
[3] V.A. Yartys, H. Fjellvåg, B.C. Hauback, A.B. Riabov, J. Alloys Compds. 274 (1998) 217.
[4] V.A. Yartys, I.Yu. Zavaliy, A.B. Riabov, P.W. Guegan, J.C. Clarke, I.R. Harris, B.C. Hauback, H. Fjellvåg, Hydrogen power: theoretical and engineering solutions, in: T.O. Saetre (Ed.), Proceedings of the International Symposium HYPOTHESIS II, Grimstad, Norway, 18–22 August 1997, Kluwer Academic Publishers, The Netherlands, 1998, 303.
[5] F. Aubertin, U. Gonser, S.J. Campbell, J. Phys. F. Met. Phys. 14 (1984) 2213.
[6] F. Aubertin, G.L. Whittle, S.J. Campbell, U. Gonser, Phys. Stat. Sol. (a) 104 (1987) 397.
[7] V.A. Yartys, H. Fjellvåg, B.C. Hauback, A.B. Riabov, M.H. Sørby, J. Alloys Compds. 278 (1–2) (1998) 252.
[8] I.Yu. Zavaliy, A.B. Riabov, V.A. Yartys, G. Wiesinger, H. Michor, G. Hilscher, J. Alloys Compds. 265 (1998) 6.
[9] I.Yu. Zavaliy, M.V. Lototzky, A.B. Riabov, V.A. Yartys, J. Alloys Compds. 219 (1995) 34.
[10] F. Gingl, K. Yvon, I.Yu. Zavaliy, V.A. Yartys, P. Fischer, J. Alloys Compds. 226 (1995) 1.
[11] P. Villars, L.D. Calvert, Pearson's Handbook of Crystallographic Data for Intermetallic Phases, 2nd ed., ASM International, Materials Park, OH, 1991.
[12] A.C. Larson, R.B. von Dreele, General Structure Analysis System, LANL, 1994.
[13] V.F. Sears, Neutron News 3 (1992) 26.
[14] A.C. Switendik, Z. Phys. Chem. NF 117 (1979) 89.
[15] V.A. Yartys, H. Fjellvåg, B.C. Hauback, A.B. Riabov, J. Alloys Comp. 287 (1999) 189.
[16] V.A. Yartys, H. Fjellvåg, B.C. Hauback, A.B. Riabov, to be published.
[17] V.A. Yartys, R. Delaplane, H. Fjellvåg, B.C. Hauback, R. McGreevy, A.B. Riabov, to be published.
[18] D. Arias, J.C. Abriata, in: T.B. Massalski et al. (Ed.), 2nd ed, Binary Alloys Phase Diagrams, Vol. 2, ASM International, USA, 1990, p. 1798.